Oxidized Bacterial Cellulose Functionalized with SiO_2 Nanoparticles as a Separator for Lithium-Metal and Lithium-Sulfur Batteries

Wenyue Li, Shu Wang, Zhaoyang Fan, Shiqi Li, Nathan Newman

W. Li, Z. Fan, School of Electrical, Computer and Energy Engineering, Arizona State University, Tempe, Arizona, 85281, USA.E-mail: zhaoyang.fan@asu.edu*

S. Wang, College of Health Solutions, Arizona State University, Phoenix, Arizona, 85004, USA.

S. Li, College of Electronic Information, Hangzhou Dianzi University, Hangzhou, 310018, China

N.Newman, School for Engineering for Matter, Transport & Energy, Arizona State University, Tempe, Arizona, 85281, USA.

Abstract:

It is highly desirable to develop lithium-metal batteries (LMBs), including lithium-sulfur batteries (LSBs), as the next-generation high-energy batteries. However, issues related to Li metal anodes and sulfur cathodes, such as non-uniform Li deposition and polysulfide shuttling, must be addressed. Here we report the study of bacterial cellulose (BC), modified by SiO_2 nanoparticles (NPs), as a separator material for LMBs and LSBs. To achieve uniform decoration of SiO_2 NPs on BC nanofibers, we oxidize and partly hydrolyze BC by introducing carboxyl groups and tetraethyl orthosilicate (TEOS). Electrochemical studies confirm that the composite BC film can smoothen the Li^+ flux, regulate the Li deposition, and curb the polysulfide shuttling due to the strong interaction of oxygen functional groups on oxidized BC and SiO_2 with Li^+ and polysulfides. As a separator used in lithium plating and stripping, the composite BC/SiO_2 film offers much better stability, lower polarization voltage, and higher Coulombic efficiency than conventional separators. When applied in Li//S and Li//$LiFePO_4$ batteries, it also demonstrates much-improved performance. Such a functionalized BC separator is very promising in LMB and LSB applications.

***Keywords**: Bacterial cellulose; separator; lithium dendrite; polysulfide shuttle; lithium-sulfur battery; lithium-metal battery*

Introduction

Elemental lithium has the highest theoretical specific capacity (3861 mAh g^{-1}) and the lowest negative potential (-3.04 V vs. standard hydrogen electrode), making it the most attractive battery anode material. Li-metal batteries (LMBs)(Cheng et al., 2017; Cheng et al., 2016; Li et al., 2014) use Li metal as the anode to substitute the conventional graphite anode of Li-ion batteries (LIBs) and a cathode based on either traditional oxide materials or more exotic sulfur(Hou et al., 2021; Zhao et al., 2018) and oxygen(Grande et al., 2015). They can deliver an energy density significantly higher than LIBs(Whittingham, 2014).

However, several challenges of using Li metal anode must be overcome before LMBs can be made available for widespread use. The formation of lithium dendrites and the associated unstable solid electrolyte interface (SEI) are the most notorious ones(Fang et al., 2019; Shen et al., 2019; Wu et al., 2018). Lithium dendrites can penetrate the separator to shorten the cathode and the anode, raising severe safety concerns(Guo et al., 2017; Wu et al., 2019a). They also can detach from the anode and form dead lithium after encapsulation by insulating SEI(Chen et al., 2017; Kushima et al., 2017; Xu et al., 2019). Moreover, the dendrite detachments expose fresh lithium to the electrolyte, causing a continuous reaction between lithium and the electrolyte, resulting in fast capacity loss and low Coulombic efficiency during battery operation(Fang et al., 2019; Liu et al., 2018).

Depending on battery chemistry, the paring cathode may exacerbate the aforementioned issues by introducing other side reactions. For example, lithium-sulfur battery (LSB) employs sulfur as the cathode material, offering several intriguing merits such as a large specific capacity (1675 mAh g^{-1}) and low cost(Li et al., 2022). However, in the stepwise conversion between S_8 and Li_2S, many intermittent lithium polysulfide species are formed, most of which are dissoluble in the electrolyte(Yen and Chung, 2021; Zhao et al., 2022). The shuttling of these polysulfides between the cathode and the anode gives rise to capacity fading, enhanced corrosion of the lithium anode, and self-discharge(Moy et al., 2014).

Lithium dendrite formation is correlated to localized high Li^+ flux "hot spots", while

the commercial polyolefin-based battery separators, with their large and non-uniform pore distribution, are one of the significant factors causing localized high Li^+ flux hot spots(Li et al., 2020b; Wang et al., 2019). Therefore, engineering the separator to facilitate uniform Li^+ transfer and Li redeposition is one promising approach to addressing the lithium dendrite problem(Liu et al., 2017; Liu et al., 2019b). In addition, reducing the separator pore size or functionalizing the separator with charged moieties can block the polysulfide pathway to curb polysulfides' shuttling effect and self-discharging in LSBs, as reported by others(Huang et al., 2015; Yu et al., 2018; Zhu et al., 2019) and ourselves(Li et al., 2021).

Therefore, engineering separators with multifunction to simultaneously address Li dendrite formation and polysulfides shuttling are attracting intense interest. For example, the periodically arranged $Co\text{-}O_4$ moieties on metal-organic framework nanosheets were synthesized as a battery separator to homogenize Li^+ flux and suppress polysulfide shuttling(Li et al., 2020c). However, building these multi-functionalized separators is challenging due to the complicated structures and synthesis methods involved. Here we report our study using bacterial cellulose (BC) anchored with SiO_2 nanoparticles (NPs) to fabricate a multi-functionalized separator.

As a natural polymer-based nanofiber network, BC offers unique properties such as strong mechanical strength, outstanding thermal and chemical stability, excellent wettability, and low cost(Huang et al., 2014; Iguchi et al., 2000). It is being investigated for use as battery separators directly or after modification/chemical functionalization(Bharti et al., 2022; Gwon et al., 2019; Huang et al., 2020; Huang et al., 2021; Kim et al., 2020; Li et al., 2021; Lokhande et al., 2022; Xie et al., 2022; Yang et al., 2020). In terms of chemical modification, the dense hydroxyl groups on cellulose chains render BC a highly polar polymer. Its dense O-containing moieties enable the formation of oxide NPs on the BC nanofibers(Araújo et al., 2018; Chanthiwong et al., 2020). A strong interaction between Li^+ and oxide NPs (and BC) helps homogenize Li^+ flux, rendering stable lithium stripping/plating. The oxygen-related bonds also effectively

absorb polysulfide species, suppressing the shuttling process(Rehman et al., 2016; Suriyakumar et al., 2018; Wu et al., 2019b).

In this work, low-cost SiO_2 is chosen as an example to modify the BC separator. It is noted SiO_2/BC structures have been reported for various applications where the structures were formed by directly mixing SiO_2 NPs and BC fibrils that causes phase segregations and clustering(Kim et al., 2020; Kim et al., 2019; Rahman et al., 2021). In contrast, our SiO_2/BC composite films were obtained *via* in-situ nucleation of SiO_2 directly on BC to achieve uniform distribution, which is crucial to homogenize the Li^+ flux in preventing lithium dendrite formation. Using such a BC/SiO_2 composite separator in the Li//Li symmetric and Li//Cu asymmetric cells to conduct the Li stripping/plating study, we observed lower polarization voltage, higher coulombic efficiency, and much longer lithium stripping/plating cycling stability when compared to cells using either the conventional Celgard 2400 (C-2400) separator or the pristine BC separator. As a result, the fabricated LSBs and Li//$LiFePO_4$ batteries had markedly improved electrochemical performances. For example, the LSB cell with 4 mg cm^{-2} of sulfur loading can deliver ~1250 mAh g^{-1} of specific capacity at 0.1C and maintain 83% capacity after 100 cycles at 0.25C. The LMB cell based on Li//$LiFePO_4$ shows high and more stable Coulombic efficiency (~99.5%) after 200 cycles. These experimental results demonstrate that the BC-based composite materials are a promising candidate for the battery separator in LMB and LSB applications.

Experimental section

BC purification and oxidation

BC pellicles produced *via* a fermentation process(Islam et al., 2017) were washed in deionized (DI) water, then boiled in 0.5 M KOH solution for one hour to remove impurities. The pellicles were then rewashed in DI water until a pH of ~7.0. To introduce carboxyl function groups into BC separators, the large BC pellicles were minced into BC

pulp and then subjected to an oxidation process(Saito et al., 2007). Briefly, 30 g of BC pulp was first dispersed into 100 mL of DI water under vigorous stirring, then 0.016 g of 2,2,6,6-tetramethylpiperidine-1-oxyl (TEMPO) and 0.1 g of NaBr were added into the solution sequentially. After they dissolved completely, 5 mL of 12% NaClO solution was added dropwise into the mixture. During the reaction process, the solution's pH was adjusted using 0.5 M NaOH to ~10. The oxidation reaction was carried out for 5 hours and then quenched by pouring 5 mL of ethanol directly into the solution. We experimented with different oxidation times to study their influence on the dispersive performance of oxidized BC (o-BC) in water. Five hours of oxidation resulted in a stable and well-mixed o-BC water suspension, avoiding sedimentation for several days. Such a stable suspension guarantees the subsequent uniform BC modification by SiO_2 NPs. The o-BC was collected *via* centrifuge and washed using 0.5 M HCl solution, DI water, and ethanol until the pH reached 7.0. The collected o-BC was homogeneously dispersed into ethanol or DI water because of their large carboxyl functional group concentration.

Fabrication of SiO_2 on oxidized BC (o-BC/SiO_2) composite films

400 μL of TEOS was dissolved into 50 mL of ethanol solution of o-BC. After stirring for 30 min, 1.0 mL of ammonium hydroxide was added dropwise into the mixture. The resulting o-BC/SiO_2 composite was collected via centrifuge, washed sequentially with DI water and ethanol, and then dispersed into 50 mL of ethanol. The o-BC/SiO_2 was separated by filtrating 25 mL of the above mixture through a PTFE membrane (44 mm diameter, 0.22 μm pore size)., the material was sandwiched between two glass slides and dried in a vacuum oven at 80 ^{o}C for 12 h to produce a flat film. The o-BC film without SiO_2 was also prepared using the same procedure.

Characterization and electrochemical test

The morphological features of the samples were studied using a field emission scanning electron microscope (FEI XL 30FE-SEM). The samples were directly attached to the sample holder using conductive tape. The images were taken under 5 kV electron accelerating voltage. X-ray diffraction (XRD) patterns of the samples were recorded in

refection mode at a step size of 0.05° by using a Rigaku MiniFlex 6G diffractometer equipped with a Cu-Kα radiation source operated at 30 kV and 15 mA. The samples were attached to a Si low background holder using double-sided tape. The collected data were corrected by subtracting the holder/tape background signals. Differential scanning calorimetry (DSC) was conducted on a LABSYS EVO instrument. Before performing the DSC measurement, the samples were dried at 80 °C in a vacuum overnight. They were loaded into a 100 μL Al_2O_3 crucible. The DSC data was recorded by heating the samples from room temperature to 600°C at a heating rate of 20 °C/min under the argon atmosphere.

To measure its Li^+ ionic conductivity, a separator was first soaked in the blank electrolyte (1 M LiTFSI in 1:1 1,3-dioxolane (DOL)/dimethylethane (DME)) and then sandwiched between two stainless steel spacers and sealed in a coin cell. Electrochemical impedance spectroscopy (EIS) test was performed to obtain the resistance, and the ionic conductivity was calculated by using the equation $\sigma = \frac{l}{RS}$, where l is the thickness of the separator, R is the resistance read from the Nyquist plot, and S is the area of the separator. The transference number t^+ was calculated using the equation of $t^+ = I_s(V - I_0R_0)/[I_0(V - I_sR_s)]$, where V is the applied DC voltage (10 mV), I_o and I_s are the initial and steady-state currents, respectively, which are read from the Chronoamperometry curves. R_o and R_s are the interfacial resistances before and after DC polarization, respectively, obtained from EIS curves.

Li//Li symmetric coin-type cells (CR2400) were fabricated by employing lithium plates as both electrodes, the C-2400 or the BC-based film as the separator, 1 M bis(trifluoromethane)sulfonamide lithium salt (LiTFSI) dissolved in a 1:1 v/v% mixture of DOL/DME solution with 1wt% $LiNO_3$ as the electrolyte. Cyclic voltammetry (CV) and EIS (0.1-100 kHz with an AC voltage amplitude of 10 mV) tests were performed on a Bio-logic SP-150 electrochemical workstation. The lithium stripping and plating cycling were recorded on a battery tester (LANHE, CT2001A). Li//Cu asymmetric cells were also characterized using a similar configuration, except a Cu foil was used for the positive

electrode.

Two different types of lithium metal batteries were chosen to demonstrate the feasibility of the o-BC/SiO_2 separator, i.e., Li//S battery and Li//$LiFePO_4$ battery. For the LSB, lithium metal was used as the anode, sulfur loaded in a carbonized BC (cBC) film as the cathode(Li et al., 2017a), the C-2400 or the BC-based film as the separator, 1 M bis(trifluoromethane)sulfonamide lithium salt (LiTFSI) with 1wt% $LiNO_3$ dissolved in a 1:1 v/v% mixture of 1,3-dioxolane (DOL)/dimethylethane (DME) solution as the electrolyte. The sulfur loading in cBC film is around 4 mg cm^{-2}, which yields sulfur weight percentage of ~65% in the cathode. The ratio of the electrolyte volume (μL) and the sulfur mass loading (mg) is ~15 μL/mg. For the Li//$LiFePO_4$ battery, a commercial $LiFePO_4$/aluminum foil (single side coated, 12 mg cm^{-2}, MTI corporation) was used as the cathode, 1 M $LiPF_6$ in ethylene carbonate (EC), and ethyl methyl carbonate (EMC) was used as the electrolyte (MTI corporation), the ratio of electrolyte and LFP is ~10μL/mg

Results and discussion

Material characterization

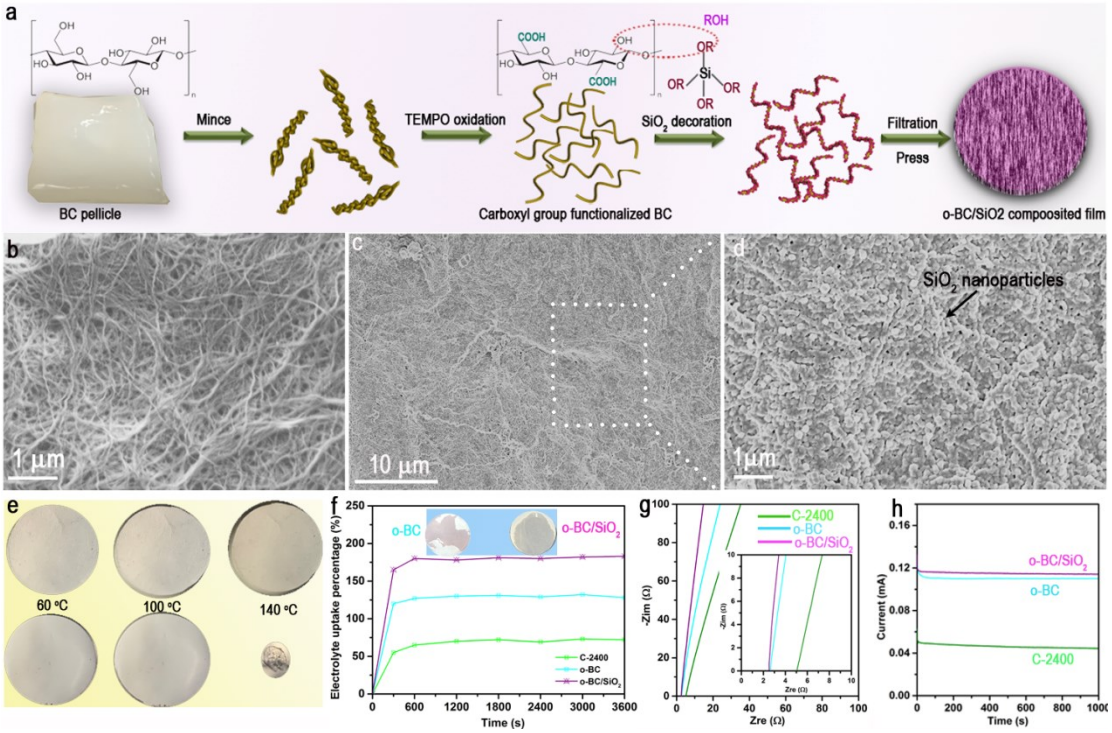

Figure 1. (a) Schematic illustration of the preparation process of the o-BC/SiO_2film. SEM image of (b) o-BC and (c and d) o-BC/SiO_2. (e) Thermal stability comparison between o-BC/SiO_2(the top line) and C-2400. (f) Electrolyte wettability and uptake capability, (g) Nyquist plots, and (h) I-t curves for the three different separator films.

Figure 1a summarizes the fabrication process for the o-BC/SiO_2 composite film. The purified BC pellicles were first minced into BC pulp and then exposed to the TEMPO oxidation process to selectively convert the C2-hydroxyl functional groups into carboxyl functional groups. The TEMPO oxidation process can also partly hydrolyze the thick fibrils into microfibrils, resulting in better dispersion in water and ethanol (Figure S1).

Previous works have reported BC materials modified with Ag, Au, and other metal nanoparticles(Chen et al., 2015; Ifuku et al., 2009; Kaushik and Moores, 2016). The distribution of the nanoparticles was significantly improved after introducing extrinsic functional groups on the BC due to the interaction between the functional groups and metal ions precursors and thinner BC fiber diameters. We imagined that a similar mechanism could also be used to produce evenly distributed metal oxides/nonmetal oxide

modified BC composites, as schematically shown in Figure 1a, where the SiO_2 precursor, TEOS(Braddock et al., 2018; Lemos et al., 2016), will react with the hydroxyl groups(Rama et al., 2019; Shafi and Zhao, 2020) and nucleate on the surface of BC nanofibrils. At the same time, the carboxyl functional groups can be preserved, which will serve as another polysulfide shuttling barrier because of the direct repulsive interaction between these carboxyl functional groups and polysulfides(Huang et al., 2021). After vacuum filtration and rolling-press steps, a BC/SiO2 composite film with controllable thickness was obtained. The SEM image of o-BC is shown in Figure 1b. The cross-linked structure guarantees the flexibility of the resulting thin film (Figure S2). The ~100 nm SiO_2 nanoparticles uniformly decorate BC nanofibrils (Figures 1c and 1d). The XRD pattern of o-BC/SiO_2 is exhibited in Figure S3. The diffraction peaks located at 2θ~14.2^o and 22.5^o can be assigned to the (101) and (002) lattice plane, respectively. The characteristic peak of amorphous SiO_2 overlaps with the o-BC at around 22°. This in-situ nucleation process shows an obvious advantage over the SiO_2/BC films fabricated by directly mixing SiO_2 nanoparticles and BC fibrils that causes phase segregations(Kim et al., 2020; Kim et al., 2019; Rahman et al., 2021).

Safe operation at high temperatures is a crucial requirement of the battery separator. The commercial Celgard membranes can only endure a temperature of ~120 ^{o}C before dangerous fault modes become prevalent during operation(Arora and Zhang, 2004; Zhang, 2007). The o-BC-based films were tested at elevated temperatures in an oven, and the results are exhibited in Figure 1e. The o-BC (not shown) and o-BC/SiO_2 films maintain structural integrity (i.e., shape and dimensions) when temperatures reach 140 ^{o}C, while the commercial C-2400 separator film melts at this temperature. To quantitatively characterize the chemical changes at elevated temperatures, a differential scanning calorimetry (DSC) method was used (Figure S4). The C-2400 separator shows a prominent endothermic peak at ~150 ^{o}C, attributed to the melting of polypropylene. In contrast, the BC-based polymer films endured temperatures as high as ~350 ^{o}C before evidence of melting or decomposition was observed. These results suggest that

incorporating BC in batteries could enable safe operation at much higher temperatures than can be achieved with the current C-2400 separator.

The electrolyte wettability and uptake capacity are critical parameters to access a film's potential for use as a battery separator. As shown in Figure 1f, with their large porosity and hydrophilicity, both o-BC and o-BC/SiO_2 films absorb more electrolytes than C-2400. A further advantage is that the wettability of o-BC can be improved significantly after being composited with SiO_2 nanoparticles (inset, Figure 1f). Table S1 summarizes the values of thickness, areal density and electrolyte uptake weight percentage of different separators, giving a clear exhibition of the merits of the oBC/SiO_2 hybrid film.

The Li^+ ionic conductivity and transference number were also measured. The experimental results are presented in Figures 1g, 1h, S5, and S6. Separators with surface functional groups such as oxygen- or nitrogen-containing groups have stronger binding energy to Li^+ (e.g., the binding energy between carbonyl and Li^+ is ~ 3.08 eV(Lin et al., 2016)) than bare separators. The Li^+ conductivities through o-BC (0.36 mS cm^{-1}) and o-BC/SiO_2 (0.39 mS cm^{-1}) films are higher than through C-2400 (0.23 mS cm^{-1}). The enhanced conductivities result from the high Li^+ affinity provided by the oxygen functional groups to both o-BC and SiO_2(Liu et al., 2019a; Pathak et al., 2019). The Li^+ transference number of o-BC-based films (0.63 for the o-BC/SiO_2 film and 0.65 for the o-BC one) is higher than that of C-2400 (0.59), suggesting its favorable Li^+ transport capability.

Li stripping and plating study

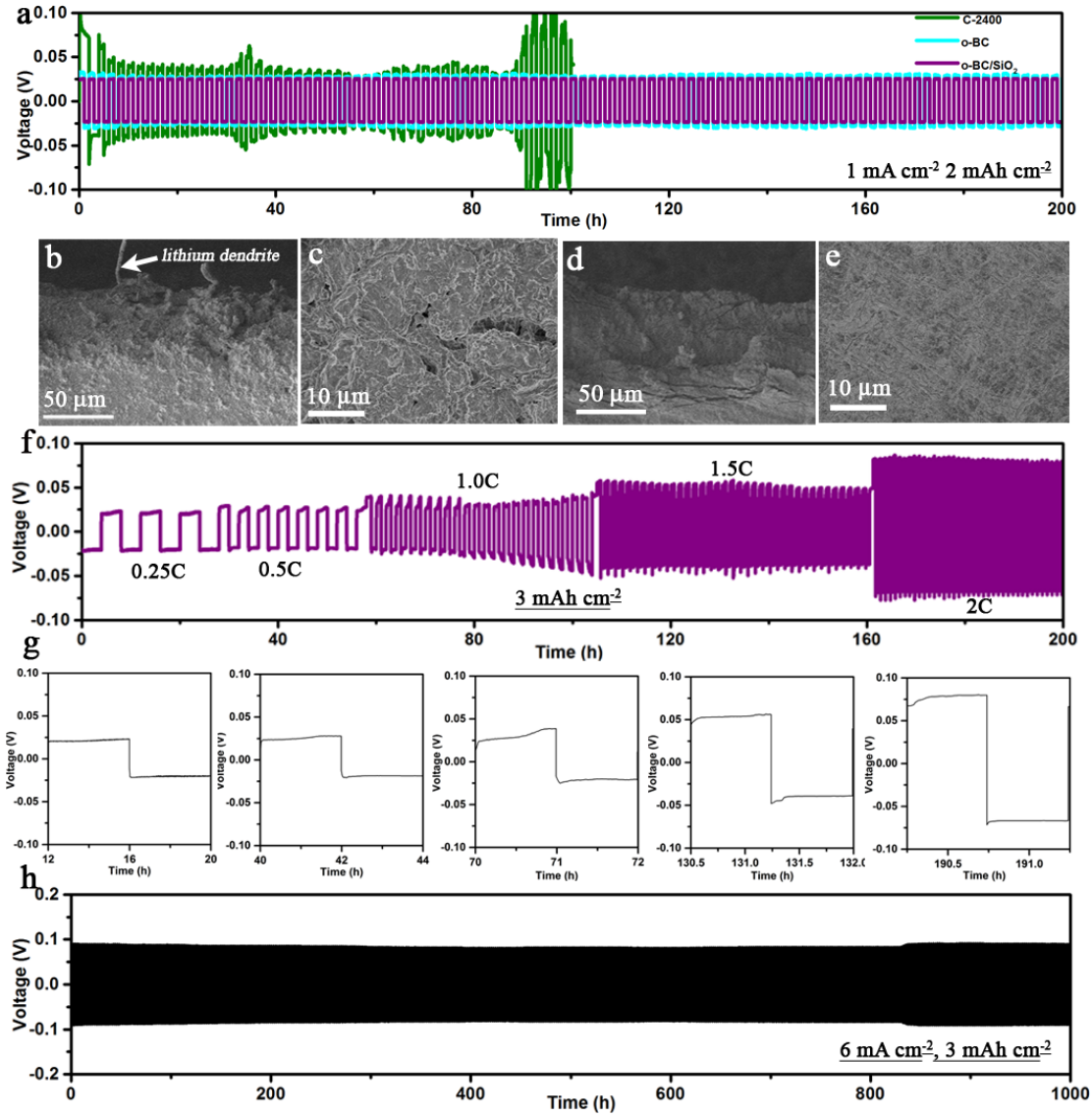

Figure 2. Lithium plating and striping result: (a) lithium stripping and plating using symmetric cells with C-2400, o-BC, or o-BC/SiO_2 film as a separator (2 mAh cm^{-2} of specific capacity and 1 mA cm^{-2} of charge/discharge current density). SEM surface and cross-sectional images of the lithium plate after lithium stripping and plating cycling (b and c: C-2400 film as the separator after 60 h, d, and e: o-BC/SiO_2film as the separator after 200 h.) (f) Rating performance of cell with the o-BC separator at 3 mAh cm^{-2} of specific capacity. (g) Charge-discharge voltage profiles under different current densities were extracted from the rating curve in Figure 2f. (h) Long-term stability test of cell with o-BC/SiO_2 separator (3 mAh $cm^{-2}$of specific capacity and 6.0 mA cm^{-2} of charge-discharge current density).

Galvanostatic cycling of Li//Li symmetric cells was performed to compare the Li stripping and plating efficiency of the commercial C-2400 with the o-BC-based separators. A cutoff potential of 120 mV was pre-set. We fixed the specific capacity to 2 mAh cm^{-2} and the charge-discharge current density to 1 mA cm^{-2}. The cells with o-BC and o-BC/SiO_2 separators exhibited very low polarization voltages (~27 and ~25 mV,

respectively) and stable cycling performance over 200 h of testing (**Figure 2a**). In contrast, the cell using a C-2400 separator suffered from a higher polarization voltage (~46 mV), which further increased to the pre-set cutoff potential of 120 mV after only 90 h.

Cycled cells were disassembled, and the structural changes in the lithium electrodes were imaged using an SEM. Figures 2b and 2c show the cross-section and surface SEM images of a lithium plate from the symmetric cell with a C-2400 separator after 60 h of testing. Lithium dendrites are visible, as indicated by the arrow in Figure 2b. The figures also show that the surface is rough and granular, the signature of non-uniform Li plating. In contrast, no lithium dendrites are observed in the lithium plate for the Li//Li cell with an o-BC/SiO_2 separator (Figure 2d). The figure also shows that the surface is smooth and uniform even after 200 h of cycling. These observations reveal that our o-BC/SiO_2 separators can more effectively regulate the lithium plating processes and suppress lithium dendrite formation and surface coarsening than the C-2400 separators. The much better performance of the o-BC/SiO_2 separator over C-2400 can be attributed to the higher Li^+ ion adsorption capability due to the more vital interaction between Li^+ and o-BC/SiO_2. The ability to absorb Li^+ by a separator in a high-rate plating process will adjust and homogenize Li^+ flux toward the plated Li electrode, resulting in uniform deposition and preventing dendrites formation and Li metal surface roughening.

Similarly, when using an o-BC film as the separator, the lithium plate is dendrite-free and very dense after cycling, without the granular and porous structure (Figure S7). The abundant oxygen functional groups on the BC are lithiophilic sites that can regulate and homogenize the Li^+ flux, leading to uniform Li deposition on the Li plate.

The stripping/plating rate performance of the Li//Li cell with the o-BC/SiO_2 separator was further evaluated, and the results are presented in Figure 2f. With the cycling current density increased from 0.75 to 6 mA cm^{-2} and maintaining the same specific capacity of 3 mAh cm^{-2}, the polarization voltage rises from ~25 to ~90 mV and then holds a relatively steady value of ~ 90 mV at 6 mA cm^{-2} during cycling. Several representative voltage

profiles under different current densities are presented in Figure 2g. The charge and discharge plateaus are smooth without any spikes for the much higher 6 mA cm^{-2} current density, reflecting stable Li^+ redox reactions on the surface of the Li electrode.

To further demonstrate the potential of the o-BC separator for fast charge-discharge and long cycling stability, the Li//Li symmetric cell was cycled at the current density of 6 mA cm^{-2} for 1000 h. As shown in Figure 2h, the overpotential maintains a value of ~90 mV for the first 850 h and then increases to ~100 mV slowly upon cycling up to the 1000th h. This excellent performance for long cycling times at large current densities demonstrates the o-BC/SiO_2 film's ability to homogenize the Li-ion flux and prohibit the dendrite formation during the Li plating process. These results further support our notion that functionalized BC-based separators have the potential to be the choice of Li metal-based battery technology in the future. The long cycling performance of the o-BC separator is presented in Figure S8. The polarization voltage stabilizes at ~100 mV at a 6 mA cm^{-2} current density for ~200 h and gradually increases to ~140 mV by the 1000th cycle.

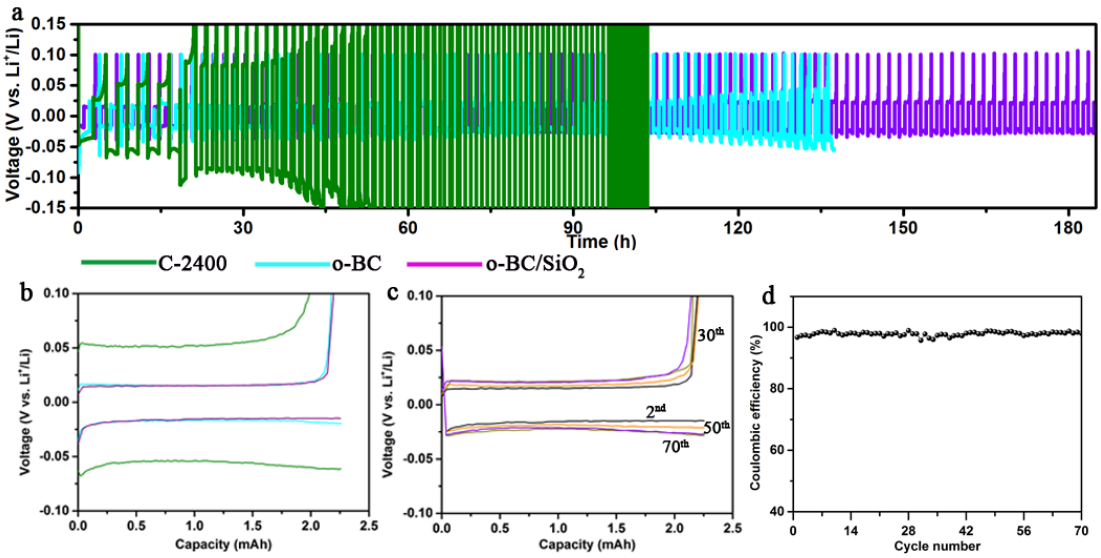

Figure 3. Li//Cu asymmetric cell testing results: (a) Cycling performance (The C-2400 and o-BC-based cells were cycled at the current density of 1.0 mA cm^{-2} at the first five cycles and the o-BC/SiO_2-based cell was cycled at the current density of 2.0 mA cm^{-2} from the beginning) and (b) Voltage profiles of cells using different separators. (c) Voltage profiles of the o-BC/SiO_2based cell at different current densities in different cycles. (d) Coulombic efficiency of the o-BC/SiO_2 based cell within 70 cycles.

To further evaluate the performance of the different separator films, we fabricated and tested asymmetric cells, which are comprised of a Li foil as the negative electrode, a copper foil as the positive electrode, and the C-2400 or the o-BC based film as the separators. For these tests, the charging cutoff voltage was set to 0.1 V. As shown in Figure 3a, with the fixed capacity of 2 mAh cm^{-2}, the C-2400 cell can only survive for a few cycles under a relatively low current density of 1.0 mA cm^{-2}. It is noted that although the cutoff voltage was set at 0.1 V during the lithium stripping process, the voltage can still jump over this limitation due to the suddenly increased large overpotential at the end of the step with no capacity recorded.

The cell with the o-BC separator exhibits a much longer lifetime, failing after ~130 h at a current density of 2 mA cm^{-2}. Overall, the o-BC/SiO_2 separators offer the best performance, as it is stable over 180 h of cycling. The voltage profiles at different capacities of the three cells are compared in Figure 3b. Cells with o-BC and o-BC/SiO_2 separators have similar polarization potential (~24 mV), significantly lower than the C-2400 cell (~50 mV). During cycling, the o-BC/SiO_2 based cell maintained its stability (Figure 3c), and Coulombic efficiency of around 98.5% was achieved (Figure 3d).

LSB and LMB performance

In addition to addressing the above Li anode issues, for Li-S batteries, shuttling of lithium polysulfides in Li-S batteries must also be inhibited to prevent low Coulombic efficiency and short battery lifetime(Li et al., 2020a; Li et al., 2015). The separator used in LSBs could help attack this problem by curbing the diffusion of polysulfides. With this in mind, the o-BC and o-BC/SiO_2 films were subjected to the polysulfides diffusion experiment, and the results are summarized in Figure 4a. All the films are shown to have the ability to block polysulfide migration at the beginning. However, polysulfides diffusion across the C-2400 film became apparent after 6 h, resulting in a color change in the left compartment. In contrast, o-BC and o-BC/SiO_2 films can successfully curb the polysulfide diffusion over 24 h of testing, a result of the strong interaction between the polysulfides and SiO_2/oxygen functional groups. Without similar active binding sites on

C-2400, it can only physically block polysulfide diffusion for a short time.

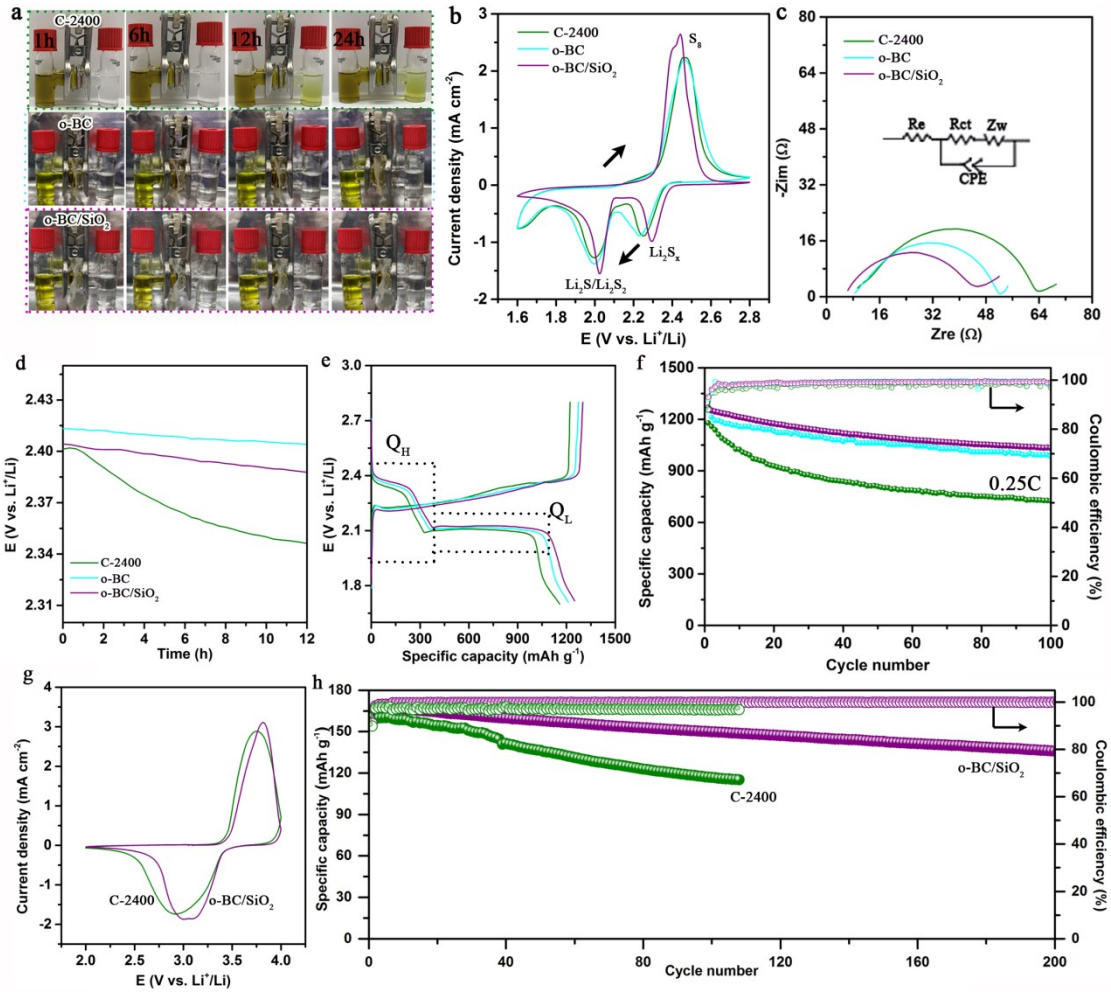

Figure 4. (a) Polysulfide diffusion results using different separators. The two compartments are isolated by the separator, with the left side being 20 mM Li_2S_6 electrolyte and the right side being a blank electrolyte). (b) CV curves recorded at 0.1 mV s^{-1}, (c) EIS Nyquist plots, and (d) open-circuit voltage (OCV) of LSB cell with different separators. (e) Voltage profiles and (f) cycling performance of different separator-based LSBs at 0.25C. (g) CV curves and (h) cycling performance of Li//$LiFePO_4$ cells with C-2400 and o-BC/SiO_2 separators.

The coin-type LSB cells with the different separators were evaluated by CV and EIS techniques. As presented in Figure 4b, all cells show three peaks located at ~2.30, 2.05, and 2.45 V originating from the conversion of S_8 to Li_2S_x (x ≥4), Li_2S_x to Li_2S/Li_2S_2, and Li_2S/Li_2S_2 to L_2S_x, respectively(Guo et al., 2013). The peak currents and potential differences between the redox peaks can be used to compare the related reaction kinetics. The o-BC/SiO_2 based LSB has the highest peak currents and smallest peak potential differences among the three cells, indicating that the o-BC/SiO_2 separator has the attractive capability to boost the redox reactions of polysulfides.

The charge transfer resistance (R_{ct}) can be derived by fitting the Nyquist plots using the equivalent circuit presented in Figure 4c. Again, the cell with o-BC/SiO_2 separator has the lowest R_{ct} of ~39 Ω, while around 55 and 44 Ω for C-2400 and o-BC based cells, respectively. These fitting results can also help to explain why the oBC/SiO_2 based LSB shows higher peak current and smaller polarization (peak current voltage difference) in comparison with oBC and C-2400-based cells.

If the shuttling process of polysulfides is not suppressed, self-discharging can become prevalent in the LSBs. After the first charging process, the open-circuit voltage (OCV) of cells with different separators was monitored for 12 h, and the results are summarized in Figure 4d. Due to the small uncontrollable differences between the freshly fabricated cells, the initial cell voltage varies (even using the same materials) and is not suitable to be used for comparing the quality of different separators. But the change of OCV along time can be employed as an indicator to study the stability (such as self-discharging) of the cells. The C-2400 cell experiences a relatively fast voltage drop from 2.41 to 2.35 V. In contrast, both o-BC and o-BC/SiO_2 based cells exhibit very stable OCV, suggesting the self-discharging, or polysulfides shuttling, has been effectively suppressed by the o-BC and o-BC/SiO_2 separators.

LSB cells with a large sulfur loading of 4 mg cm^{-2} were assembled to verify the function of BC-derived separators in improving battery performance. A carbonized BC nanofiber film loaded with sulfur was used for the cathode because it offers highly conductive networks and abundant surfaces for sulfur/polysulfides to attach(Li et al., 2017a; Li et al., 2017b). These cells were cycled at 0.25C for 100 cycles. As illustrated in Figures 4e and 4f, the cell using an o-BC/SiO_2 separator delivers a larger capacity during discharge, with both higher Q_H that corresponds to the discharge capacity for S_8 to Li_2S_x conversion and Q_L that corresponds to Li_2S_x to Li_2S/Li_2S_2 conversion, than the o-BC-based and the C-2400-based cells. The trend of discharge capacity variation of the three cells is consistent with our expectations based on the CV results. During cycling, the C-2400 cell shows a faster specific capacity decay than the other two and maintains a

capacity of ~740 mAh g^{-1} up to the 100th cycle. Comparatively, the cell with o-BC or o-BC/SiO_2 can still deliver ~1000 mAh g^{-1} of capacity up to the 100th cycle (~ 985 mAh g^{-1} for the o-BC cell and ~1033 mAh g^{-1} for the o-BC/SiO_2 cell). In addition, the o-BC/SiO_2 cell also exhibits higher Coulombic efficiency (> 99%) than its counterparts.

Li//$LiFePO_4$ cells with C-2400 and o-BC/SiO_2 separators were also assembled and tested. Figure 4f presents the CV curves recorded between 2.0 and 4.0 V at a scan rate of 0.1 mV s^{-1}. The redox peak currents and peak potential differences of the o-BC/SiO_2 based cell are also superior to those of the C-2400 based cell. When both cells are cycled at 0.2C, the one with the C-2400 separator suffers from quicker capacity decay and lower coulombic efficiency. These results are consistent with the previously reported unmodified $LiFePO_4$-based cells with Celgard separators(Chang et al., 2008; Deng et al., 2022). Although the o-BC/SiO_2 cell also shows a specific capacity decrease during cycling, it only slowly decreases from the initial value of 165 to 136 mAh g^{-1} after 200 cycles, again demonstrating the capability of the o-BC/SiO_2 separator in improving the battery performance. The improved performance is attributed to the capability of SiO_2 functionalized BC to regulate the Li^+ flux to the anode during the Li deposition. A uniform Li deposition on the anode can lower the overpotential and suppress the battery degradation caused by the dead lithium and lithium dendrites.

Conclusions

The main goal of the work reported here is to engineer separators so that lithium metal anodes can be used to make practical LMBs for wide spread use. Electrochemical studies show that the composite o-BC/SiO_2 separator that we developed can(1) generate a smooth Li^+ flux, (2) regulate the Li deposition, and (3) curb the polysulfide shuttling process as a result of the strong interaction between oxygen functional groups on oxidized BC and SiO_2 with Li^+ and polysulfides. When such a composite film was used as the separator in lithium plating and stripping, much better stability, lower polarization voltage, and higher Coulombic efficiency were achieved than conventional separators. Benefiting

from the oxidation process implemented on pristine BC, the introduced carboxylate groups can effectively modify the SiO_2 growth process resulting in a uniform coating on BC. We expected using similar methods, other nonmetal or metal oxides/sulfides materials can also be introduced uniformly onto the BC fibers, which may lead to better structure and composition for the separator used in LMB or other batteries.

Ethics approval and consent to participate

Not applicable.

Consent for publication

Not applicable.

Availability of data and materials

Not applicable.

Competing interests

The authors declare the following financial interests/personal relationships which may be considered as potential competing interests: ZF, WL, and SW have a patent pending to Arizona State University.

Funding

National Science Foundation of U.S.A (2103582, 2129983).

Authors' contributions

Wenyue Li: Conceptualization, Methodology, Investigation, Writing. Shu Wang: Conceptual, Resources, Writing. Zhaoyang Fan: Conceptualization, Methodology, Writing, Supervision. Shiqi Li: Resources. Nathan Newman: Resources, Writing.

Acknowledgements

This work at Arizona State University was supported by the National Science Foundation of U.S.A (2103582, 2129983).

Authors' information

Authors and Affiliations

School of Electrical, Computer and Energy Engineering, Arizona State University, Tempe, Arizona, 85281, USA.

Wenyue Li, Zhaoyang Fan

College of Health Solutions, Arizona State University, Phoenix, Arizona, 85004, USA.

Shu Wang

College of Electronic Information, Hangzhou Dianzi University, Hangzhou, 310018, China

Shiqi Li

School for Engineering for Matter, Transport & Energy, Arizona State University, Tempe, Arizona, 85281, USA.

Nathan Newman

Corresponding author: Zhaoyang Fan, E-mail: zhaoyang.fan@asu.edu

References

Araújo, I.M., Silva, R.R., Pacheco, G., Lustri, W.R., Tercjak, A., Gutierrez, J., Júnior, J.R., Azevedo, F.H., Figuêredo, G.S., Vega, M.L., 2018. Hydrothermal synthesis of bacterial cellulose–copper oxide nanocomposites and evaluation of their antimicrobial activity. Carbohydrate polymers 179, 341-349.

Arora, P., Zhang, Z., 2004. Battery separators. Chemical reviews 104, 4419-4462.

Bharti, V.K., Pathak, A.D., Sharma, C.S., Khandelwal, M., 2022. Flexible and free-standing bacterial cellulose derived cathode host and separator for lithium-sulfur batteries. Carbohydrate Polymers 293, 119731.

Braddock, D.C., Lickiss, P.D., Rowley, B.C., Pugh, D., Purnomo, T., Santhakumar, G., Fussell, S.J., 2018. Tetramethyl orthosilicate (TMOS) as a reagent for direct amidation of carboxylic acids. Organic letters 20, 950-953.

Chang, H.-H., Chang, C.-C., Su, C.-Y., Wu, H.-C., Yang, M.-H., Wu, N.-L., 2008. Effects of TiO2 coating on high-temperature cycle performance of LiFePO4-based lithium-ion batteries. Journal of Power Sources 185, 466-472.

Chanthiwong, M., Mongkolthanaruk, W., Eichhorn, S.J., Pinitsoontorn, S., 2020. Controlling the processing of co-precipitated magnetic bacterial cellulose/iron oxide nanocomposites. Materials & Design 196, 109148.

Chen, K.-H., Wood, K.N., Kazyak, E., LePage, W.S., Davis, A.L., Sanchez, A.J., Dasgupta, N.P., 2017. Dead lithium: mass transport effects on voltage, capacity, and failure of lithium metal anodes. Journal of Materials Chemistry A 5, 11671-11681.

Chen, M., Kang, H., Gong, Y., Guo, J., Zhang, H., Liu, R., 2015. Bacterial cellulose supported gold nanoparticles with excellent catalytic properties. ACS Applied Materials & Interfaces 7, 21717-21726.

Cheng, X.-B., Zhang, R., Zhao, C.-Z., Zhang, Q., 2017. Toward safe lithium metal anode in rechargeable batteries: a review. Chemical reviews 117, 10403-10473.

Cheng, X.B., Zhang, R., Zhao, C.Z., Wei, F., Zhang, J.G., Zhang, Q., 2016. A review of solid electrolyte interphases on lithium metal anode. Advanced science 3, 1500213.

Deng, J., Cao, D., Yang, X., Zhang, G., 2022. Cross-linked cellulose/carboxylated polyimide nanofiber separator for lithium-ion battery application. Chemical Engineering Journal 433, 133934.

Fang, C., Wang, X., Meng, Y.S., 2019. Key issues hindering a practical lithium-metal anode. Trends in Chemistry 1, 152-158.

Grande, L., Paillard, E., Hassoun, J., Park, J.B., Lee, Y.J., Sun, Y.K., Passerini, S., Scrosati, B., 2015. The lithium/air battery: still an emerging system or a practical reality? Advanced materials 27, 784-800.

Guo, J., Yang, Z., Yu, Y., Abruña, H.c.D., Archer, L.A., 2013. Lithium–sulfur battery cathode enabled by lithium–nitrile interaction. Journal of the American Chemical Society 135, 763-767.

Guo, Y., Li, H., Zhai, T., 2017. Reviving lithium‐metal anodes for next‐generation high‐energy batteries. Advanced materials 29, 1700007.

Gwon, H., Park, K., Chung, S.-C., Kim, R.-H., Kang, J.K., Ji, S.M., Kim, N.-J., Lee, S., Ku, J.-H., Do, E.C., 2019. A safe and sustainable bacterial cellulose nanofiber separator for lithium rechargeable batteries. Proceedings of the National Academy of Sciences 116, 19288-19293.

Hou, L.-P., Zhang, X.-Q., Li, B.-Q., Zhang, Q., 2021. Challenges and promises of lithium metal anode by soluble polysulfides in practical lithium–sulfur batteries. Materials Today 45, 62-76.

Huang, C., Ji, H., Yang, Y., Guo, B., Luo, L., Meng, Z., Fan, L., Xu, J., 2020. TEMPO-oxidized bacterial cellulose nanofiber membranes as high-performance separators for lithium-ion batteries. Carbohydrate polymers 230, 115570.

Huang, J.-Q., Zhang, Q., Wei, F., 2015. Multi-functional separator/interlayer system for high-stable lithium-sulfur batteries: Progress and prospects. Energy Storage Materials 1, 127-145.

Huang, Q., Zhao, C., Li, X., 2021. Enhanced electrolyte retention capability of separator for lithium-ion battery constructed by decorating ZIF-67 on bacterial cellulose nanofiber. Cellulose 28, 3097-3112.

Huang, Y., Zhu, C., Yang, J., Nie, Y., Chen, C., Sun, D., 2014. Recent advances in bacterial

cellulose. Cellulose 21, 1-30.
Ifuku, S., Tsuji, M., Morimoto, M., Saimoto, H., Yano, H., 2009. Synthesis of silver nanoparticles templated by TEMPO-mediated oxidized bacterial cellulose nanofibers. Biomacromolecules 10, 2714-2717.
Iguchi, M., Yamanaka, S., Budhiono, A., 2000. Bacterial cellulose—a masterpiece of nature's arts. Journal of materials science 35, 261-270.
Islam, N., Li, S., Ren, G., Zu, Y., Warzywoda, J., Wang, S., Fan, Z., 2017. High-frequency electrochemical capacitors based on plasma pyrolyzed bacterial cellulose aerogel for current ripple filtering and pulse energy storage. Nano Energy 40, 107-114.
Kaushik, M., Moores, A., 2016. Nanocelluloses as versatile supports for metal nanoparticles and their applications in catalysis. Green Chemistry 18, 622-637.
Kim, H., Mattinen, U., Guccini, V., Liu, H., Salazar-Alvarez, G., Lindström, R.W., Lindbergh, G.r., Cornell, A., 2020. Feasibility of chemically modified cellulose nanofiber membranes as lithium-ion battery separators. ACS applied materials & interfaces 12, 41211-41222.
Kim, U.-J., Kimura, S., Wada, M., 2019. Facile preparation of cellulose-SiO2 composite aerogels with high SiO2 contents using a LiBr aqueous solution. Carbohydrate polymers 222, 114975.
Kushima, A., So, K.P., Su, C., Bai, P., Kuriyama, N., Maebashi, T., Fujiwara, Y., Bazant, M.Z., Li, J., 2017. Liquid cell transmission electron microscopy observation of lithium metal growth and dissolution: Root growth, dead lithium and lithium flotsams. Nano Energy 32, 271-279.
Lemos, E.M., Patrício, P.S., Pereira, M.M., 2016. 3D nanocomposite chitosan/bioactive glass scaffolds obtained using two different routes: an evaluation of the porous structure and mechanical properties. Química Nova 39, 462-466.
Li, M.-C., Liu, Z., Tan, L., Zhou, Q.-Y., Zhang, J.-J., Hou, P.-P., Jin, X.-J., Lv, T.-B., Zhao, Z.-Q., Zeng, Z., 2022. Fabrication of Cubic and Porous Carbon Cages with In-Situ-Grown Carbon Nanotube Networks and Cobalt Phosphide for High-Capacity and Stable Lithium–Sulfur Batteries. ACS Sustainable Chemistry & Engineering 10, 10223-10233.
Li, S., Leng, D., Li, W., Qie, L., Dong, Z., Cheng, Z., Fan, Z., 2020a. Recent progress in developing Li2S cathodes for Li–S batteries. Energy Storage Materials 27, 279-296.
Li, S., Mou, T., Ren, G., Warzywoda, J., Wei, Z., Wang, B., Fan, Z., 2017a. Gel based sulfur cathodes with a high sulfur content and large mass loading for high-performance lithium–sulfur batteries. Journal of Materials Chemistry A 5, 1650-1657.
Li, S., Warzywoda, J., Wang, S., Ren, G., Fan, Z., 2017b. Bacterial cellulose derived carbon nanofiber aerogel with lithium polysulfide catholyte for lithium–sulfur batteries. Carbon 124, 212-218.
Li, W., Wang, S., Fan, Z., Li, S., Bernussi, A., Newman, N., 2021. Functionalized bacterial cellulose as a separator to address polysulfides shuttling in lithium–sulfur batteries. Materials Today Energy 21, 100813.
Li, W., Yao, H., Yan, K., Zheng, G., Liang, Z., Chiang, Y.-M., Cui, Y., 2015. The synergetic effect of lithium polysulfide and lithium nitrate to prevent lithium dendrite growth. Nature communications 6, 1-8.
Li, Y., Cao, D., Arnold, W., Ren, Y., Liu, C., Jasinski, J.B., Druffel, T., Cao, Y., Zhu, H., Wang, H., 2020b. Regulated lithium ionic flux through well-aligned channels for lithium dendrite inhibition in solid-state batteries. Energy Storage Materials 31, 344-351.
Li, Y., Lin, S., Wang, D., Gao, T., Song, J., Zhou, P., Xu, Z., Yang, Z., Xiao, N., Guo, S., 2020c. Single atom array mimic on ultrathin MOF nanosheets boosts the safety and life of lithium–sulfur batteries. Advanced Materials 32, 1906722.
Li, Z., Huang, J., Liaw, B.Y., Metzler, V., Zhang, J., 2014. A review of lithium deposition in lithium-ion and lithium metal secondary batteries. Journal of power sources 254, 168-182.
Lin, D., Liu, Y., Liang, Z., Lee, H.-W., Sun, J., Wang, H., Yan, K., Xie, J., Cui, Y., 2016. Layered reduced graphene oxide with nanoscale interlayer gaps as a stable host for lithium metal anodes. Nature nanotechnology 11, 626-632.
Liu, B., Zhang, J.-G., Xu, W., 2018. Advancing lithium metal batteries. Joule 2, 833-845.
Liu, W., Mi, Y., Weng, Z., Zhong, Y., Wu, Z., Wang, H., 2017. Functional metal–organic framework boosting lithium metal anode performance via chemical interactions. Chemical science 8, 4285-4291.
Liu, Y., Qin, X., Zhang, S., Huang, Y., Kang, F., Chen, G., Li, B., 2019a. Oxygen and nitrogen co-doped porous carbon granules enabling dendrite-free lithium metal anode. Energy Storage Materials 18, 320-327.
Liu, Y., Xiong, S., Wang, J., Jiao, X., Li, S., Zhang, C., Song, Z., Song, J., 2019b. Dendrite-free lithium metal anode enabled by separator engineering via uniform loading of lithiophilic nucleation sites. Energy Storage Materials 19, 24-30.
Lokhande, P., Singh, P.P., Vo, D.-V.N., Kumar, D., Balasubramanian, K., Mubayi, A., Srivastava,

A., Sharma, A., 2022. Bacterial Nanocellulose: Green Polymer Materials for High Performance Energy Storage Applications. Journal of Environmental Chemical Engineering, 108176.
Moy, D., Manivannan, A., Narayanan, S., 2014. Direct measurement of polysulfide shuttle current: a window into understanding the performance of lithium-sulfur cells. Journal of the electrochemical society 162, A1.
Pathak, R., Chen, K., Gurung, A., Reza, K.M., Bahrami, B., Wu, F., Chaudhary, A., Ghimire, N., Zhou, B., Zhang, W.H., 2019. Ultrathin bilayer of graphite/SiO2 as solid interface for reviving Li metal anode. Advanced Energy Materials 9, 1901486.
Rahman, K.U., Ferreira-Neto, E.P., Rahman, G.U., Parveen, R., Monteiro, A.S., Rahman, G., Van Le, Q., Domeneguetti, R.R., Ribeiro, S.J., Ullah, S., 2021. Flexible bacterial cellulose-based BC-SiO2-TiO2-Ag membranes with self-cleaning, photocatalytic, antibacterial and UV-shielding properties as a potential multifunctional material for combating infections and environmental applications. Journal of Environmental Chemical Engineering 9, 104708.
Rama, S., Zhang, Y., Tchuenbou-Magaia, F., Ding, Y., Li, Y., 2019. Encapsulation of 2-amino-2-methyl-1-propanol with tetraethyl orthosilicate for CO 2 capture. Frontiers of Chemical Science and Engineering 13, 672-683.
Rehman, S., Guo, S., Hou, Y., 2016. Rational design of Si/SiO2@ hierarchical porous carbon spheres as efficient polysulfide reservoirs for high‐performance Li–S battery. Advanced materials 28, 3167-3172.
Saito, T., Kimura, S., Nishiyama, Y., Isogai, A., 2007. Cellulose nanofibers prepared by TEMPO-mediated oxidation of native cellulose. Biomacromolecules 8, 2485-2491.
Shafi, S., Zhao, Y., 2020. Superhydrophobic, enhanced strength and thermal insulation silica aerogel/glass fiber felt based on methyltrimethoxysilane precursor and silica gel impregnation. Journal of Porous Materials 27, 495-502.
Shen, K., Wang, Z., Bi, X., Ying, Y., Zhang, D., Jin, C., Hou, G., Cao, H., Wu, L., Zheng, G., 2019. Magnetic Field–Suppressed Lithium Dendrite Growth for Stable Lithium‐Metal Batteries. Advanced Energy Materials 9, 1900260.
Suriyakumar, S., Stephan, A.M., Angulakshmi, N., Hassan, M.H., Alkordi, M.H., 2018. Metal–organic framework@ SiO 2 as permselective separator for lithium–sulfur batteries. Journal of Materials Chemistry A 6, 14623-14632.
Wang, C., Wang, A., Ren, L., Guan, X., Wang, D., Dong, A., Zhang, C., Li, G., Luo, J., 2019. Controlling Li ion flux through materials innovation for dendrite‐free lithium metal anodes. Advanced Functional Materials 29, 1905940.
Whittingham, M.S., 2014. Ultimate limits to intercalation reactions for lithium batteries. Chemical reviews 114, 11414-11443.
Wu, B., Yang, Y., Liu, D., Niu, C., Gross, M., Seymour, L., Lee, H., Le, P.M., Vo, T.D., Deng, Z.D., 2019a. Good practices for rechargeable lithium metal batteries. Journal of The Electrochemical Society 166, A4141.
Wu, F., Yuan, Y.-X., Cheng, X.-B., Bai, Y., Li, Y., Wu, C., Zhang, Q., 2018. Perspectives for restraining harsh lithium dendrite growth: Towards robust lithium metal anodes. Energy Storage Materials 15, 148-170.
Wu, J., You, N., Li, X., Zeng, H., Li, S., Xue, Z., Ye, Y., Xie, X., 2019b. SiO 2@ MoS 2 core–shell nanocomposite layers with high lithium ion diffusion as a triple polysulfide shield for high performance lithium–sulfur batteries. Journal of Materials Chemistry A 7, 7644-7653.
Xie, Y., Zhu, H., Zeng, R., Na, B., Zou, S., Chen, C., 2022. Chemical foaming integrated polydopamine hybridization towards high-performance cellulose-based separators for ultrastable and high-rate lithium metal batteries. Journal of Power Sources 538, 231562.
Xu, S., Chen, K.-H., Dasgupta, N.P., Siegel, J.B., Stefanopoulou, A.G., 2019. Evolution of Dead Lithium Growth in Lithium Metal Batteries: Experimentally Validated Model of the Apparent Capacity Loss. Journal of The Electrochemical Society 166, A3456.
Yang, Y., Huang, C., Gao, G., Hu, C., Luo, L., Xu, J., 2020. Aramid nanofiber/bacterial cellulose composite separators for lithium-ion batteries. Carbohydrate polymers 247, 116702.
Yen, Y.-J., Chung, S.-H., 2021. Lean-electrolyte lithium–sulfur electrochemical cells with high-loading carbon nanotube/nanofiber–polysulfide cathodes. Chemical Communications 57, 2009-2012.
Yu, X., Feng, S., Boyer, M.J., Lee, M., Ferrier Jr, R.C., Lynd, N.A., Hwang, G.S., Wang, G., Swinnea, S., Manthiram, A., 2018. Controlling the polysulfide diffusion in lithium-sulfur batteries with a polymer membrane with intrinsic nanoporosity. Materials today energy 7, 98-104.
Zhang, S.S., 2007. A review on the separators of liquid electrolyte Li-ion batteries. Journal of power sources 164, 351-364.
Zhao, H., Deng, N., Yan, J., Kang, W., Ju, J., Ruan, Y., Wang, X., Zhuang, X., Li, Q., Cheng, B.,

2018. A review on anode for lithium-sulfur batteries: Progress and prospects. Chemical Engineering Journal 347, 343-365.

Zhao, T., Chen, J., Dai, K., Zhang, J., Yuan, M., Li, X., Zhang, K., Zhang, J., Li, Y., Liu, Z., 2022. Boosted polysulfides regulation by iron carbide nanoparticles-embedded porous biomass-derived carbon toward superior lithium–sulfur batteries. Journal of Colloid and Interface Science 605, 129-137.

Zhu, X., Ouyang, Y., Chen, J., Zhu, X., Luo, X., Lai, F., Zhang, H., Miao, Y.-E., Liu, T., 2019. In situ extracted poly (acrylic acid) contributing to electrospun nanofiber separators with precisely tuned pore structures for ultra-stable lithium–sulfur batteries. Journal of Materials Chemistry A 7, 3253-3263.